


Article

The Utility of ADC First-Order Histogram Features for the Prediction of Metachronous Metastases in Rectal Cancer: A Preliminary Study

Bianca Boca (Petresc)^{1,2,3} , Cosmin Caraiani^{3,4,*}, Loredana Popa^{3,*}, Andrei Lebovici^{2,5}, Diana Sorina Feier^{2,5}, Carmen Bodale^{6,7} and Mircea Marian Buruian¹

- ¹ Department of Radiology, “George Emil Palade” University of Medicine, Pharmacy, Science and Technology of Târgu Mureș, 540139 Târgu Mureș, Romania; petresc.bianca@elearn.umfcluj.ro (B.B.); mircea.buruian@umfst.ro (M.M.B.)
- ² Department of Radiology, Emergency Clinical County Hospital Cluj-Napoca, 400006 Cluj-Napoca, Romania; andrei.lebovici@umfcluj.ro (A.L.); diana.feier@umfcluj.ro (D.S.F.)
- ³ Department of Medical Imaging, “Iuliu Hațieganu” University of Medicine and Pharmacy Cluj-Napoca, 400012 Cluj-Napoca, Romania
- ⁴ Department of Radiology, Regional Institute of Gastroenterology and Hepatology “Prof. Dr. Octavian Fodor”, 400158 Cluj-Napoca, Romania
- ⁵ Department of Radiology, “Iuliu Hațieganu” University of Medicine and Pharmacy Cluj-Napoca, 400012 Cluj-Napoca, Romania
- ⁶ Department of Oncology, Amethyst Radiotherapy Center Cluj, 407280 Florești, Romania; carmen.bodale@amethyst-radiotherapy.com
- ⁷ Department of Medical Oncology and Radiotherapy, “Iuliu Hațieganu” University of Medicine and Pharmacy Cluj-Napoca, 400012 Cluj-Napoca, Romania
- * Correspondence: cosmin.caraiani@umfcluj.ro (C.C.); loredana.popa@elearn.umfcluj.ro (L.P.)



Citation: Boca, B.; Caraiani, C.; Popa, L.; Lebovici, A.; Feier, D.S.; Bodale, C.; Buruian, M.M. The Utility of ADC First-Order Histogram Features for the Prediction of Metachronous Metastases in Rectal Cancer: A Preliminary Study. *Biology* **2022**, *11*, 452. <https://doi.org/10.3390/biology11030452>

Academic Editor: Pilar Roca

Received: 31 December 2021

Accepted: 14 March 2022

Published: 16 March 2022

Publisher’s Note: MDPI stays neutral with regard to jurisdictional claims in published maps and institutional affiliations.



Copyright: © 2022 by the authors. Licensee MDPI, Basel, Switzerland. This article is an open access article distributed under the terms and conditions of the Creative Commons Attribution (CC BY) license (<https://creativecommons.org/licenses/by/4.0/>).

Simple Summary: Metachronous metastases are the main factors affecting survival in rectal cancer, and 15–25% of patients will develop them at a 5-year follow-up. Early identification of patients with higher risk of developing distant metachronous metastases would help to improve therapeutic protocols and could allow for a more accurate, personalized management. Apparent diffusion coefficient (ADC) represents an MRI quantitative biomarker, which can assess the diffusion characteristics of tissues, depending on the microscopic mobility of water, showing information related to tissue cellularity. First-order histogram-based features statistics describe the frequency distribution of intensity values within a region of interest, revealing microstructural alterations. In our study, we demonstrated that whole-tumor ADC first-order features may provide useful information for the assessment of rectal cancer prognosis, regarding the occurrence of metachronous metastases.

Abstract: This study aims the ability of first-order histogram-based features, derived from ADC maps, to predict the occurrence of metachronous metastases (MM) in rectal cancer. A total of 52 patients with pathologically confirmed rectal adenocarcinoma were retrospectively enrolled and divided into two groups: patients who developed metachronous metastases ($n = 15$) and patients without metachronous metastases ($n = 37$). We extracted 17 first-order (FO) histogram-based features from the pretreatment ADC maps. Student’s t -test and Mann-Whitney U test were used for the association between each FO feature and presence of MM. Statistically significant features were combined into a model, using the binary regression logistic method. The receiver operating curve analysis was used to determine the diagnostic performance of the individual parameters and combined model. There were significant differences in ADC 90th percentile, interquartile range, entropy, uniformity, variance, mean absolute deviation, and robust mean absolute deviation in patients with MM, as compared to those without MM (p values between 0.002–0.01). The best diagnostic was achieved by the 90th percentile and uniformity, yielding an AUC of 0.74 [95% CI: 0.60–0.8]). The combined model reached an AUC of 0.8 [95% CI: 0.66–0.90]. Our observations point out that ADC first-order features may be useful for predicting metachronous metastases in rectal cancer.

Keywords: rectal cancer; magnetic resonance imaging; apparent diffusion coefficient; metachronous metastases; first-order features; histogram

1. Introduction

Colorectal cancer is one of the most frequent cancers worldwide, occupying the third position, in terms of incidence and the second place, in terms of mortality [1,2]. Approximately 30–35% of all colorectal tumors are represented by rectal cancers (RC) [2,3]. The current standard treatment for locally advanced rectal cancer (LARC) is neoadjuvant chemoradiotherapy (nCRT), followed by surgery with total mesorectal excision (TME) [4,5]. However, studies report that nCRT has no effect on overall survival [6,7]. Recurrence, in the form of distant metastases, is the main factor affecting the overall survival rate, with 15–25% of patients diagnosed with rectal cancer having developed distant metastases (DM) by the 5-year follow-up [8–10]. Therefore, identification of patients with a high risk of developing distant metachronous metastases is a major concern, especially since there is still controversy around the use of adjuvant chemotherapy to improve disease-free survival [11–16].

Recent papers have focused on rectal cancer prognosis, investigating both clinico-pathological and medical imaging factors as possible predictors of different outcomes. TNM staging, histological grade, extramural vascular invasion (EMVI), neural invasion, circumferential margin (CRM) involvement, pretreatment serum level of carcinoembryonic antigen (CEA), and pathological responses to nCRT have been identified as powerful prognostic factors [17–20]. Increased intratumoral heterogeneity may also represent a potential prognostic factor [21,22], which can be quantified using different imaging parameters, including several derived from magnetic resonance imaging (MRI) [23].

Diffusion weighted imaging (DWI) is a functional MRI technique, based on the Brownian movement of water molecules in tissues, which can be quantified using apparent diffusion coefficient (ADC). ADC values, expressed in units of mm^2/s , are displayed as a parametric map (ADC map) that reflects the degree of diffusion of water molecules through different tissues. Studies demonstrated a negative correlation between ADC and tissue characteristics, such as cellularity or proliferation activity [24,25], turning it into a promising biomarker of tumor aggressiveness. As for rectal cancer, many papers have investigated the role of ADC mean values to predict histopathological features and response to nCRT [26]. However, according to a recent meta-analysis, their conclusions are inconsistent [26].

First-order statistical parameters are quantitative features derived from the gray-level intensity histograms, which describe the distribution of signal intensity values within a region or volume of interest (VOI). Voxel-based histogram analysis of a VOI can assess the whole tumor volume and offer an objective overview of tumor heterogeneity [23,27]. Recent studies have used histogram analysis in different areas of cancer research, including rectal cancer [28–32].

The aim of the present study was to investigate the value of first-order histogram-based features derived from pre-treatment ADC maps for the prediction of distant metachronous metastases of rectal tumors.

2. Materials and Methods

2.1. Study Population

The local institutional ethics committee approved this study and informed consent was waived, due to the retrospective nature of the study. A retrospective analysis was conducted in our electronic medical database for patients diagnosed with rectal cancer who underwent an MR examination for initial tumor staging between January 2017 and May 2019. The inclusion criteria were: patients with pathologically confirmed rectal adenocarcinoma, no evidence of metastatic disease at the baseline computed tomography (CT) scan, and oncologic follow-up with CT scan of chest, abdomen, and pelvis, within at least 1 year after

the initial tumor staging. The exclusion criteria were as follows: MR examinations with severe artifacts and insufficient quality for proper analysis (15 patients), pathologically confirmed mucinous adenocarcinoma (10 patients), pathologically confirmed anal cancer (3 patients), lack of baseline CT (7 patients), synchronous metastases (16 patients), and incomplete oncologic follow-up data (49 patients). Our final study population consisted of 52 eligible patients. All subjects underwent curative surgery, most of them receiving neoadjuvant chemoradiotherapy before the intervention (48 patients). The clinical follow-up examinations were performed every three months in the first two years and every six months in the following two years and included physical examination, carcinoembryonic antigen testing, and imaging with CT or MRI/PET, when recommended. The study population was divided into two groups: patients who developed metachronous metastases (15 patients) and patients without metachronous metastases (37 patients). Metachronous metastases (MM) were considered any distant metastases, which were diagnosed at a follow-up CT examination, performed after the baseline CT for initial staging.

2.2. Image Acquisition

All MRI rectal examinations were performed in a single institution, using a 1.5 Tesla MRI scanner (Magnetom Essenza, Siemens AG, Erlangen, Germany), with an eight-channel phased array body coil. The protocol included three T2 weighted turbo spin-echo (TSE) sequences in the sagittal, oblique-axial high-resolution, and oblique coronal high-resolution planes. DWI images were obtained in axial planes using EPI sequences at three b-values (b50, b400, and b800 s/mm²). Apparent diffusion coefficient (ADC) maps were automatically generated by the scanner software, using all three b values (Figure 1). ADC values are expressed in 10⁻⁶ mm²/s.

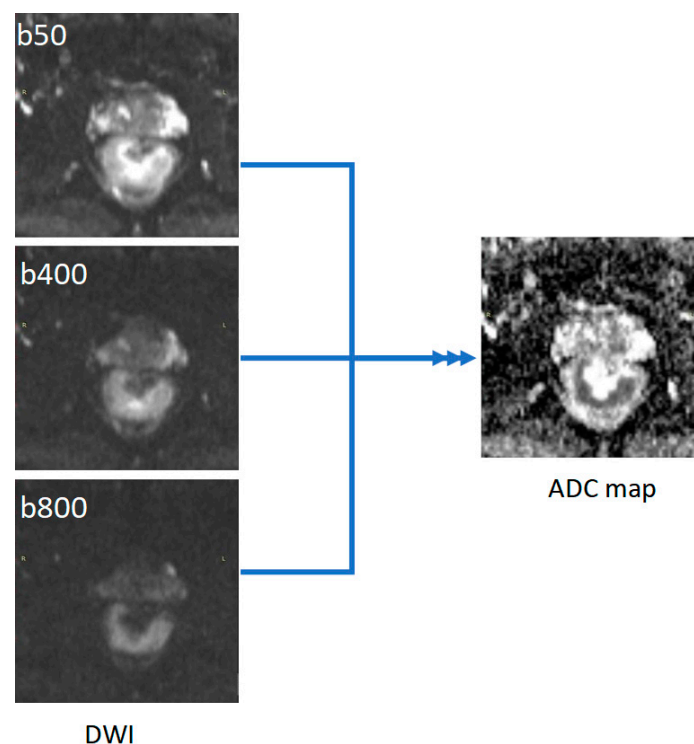


Figure 1. Example of ADC map generated from DWI images with three b values (50, 400, and 800).

The parameters of the MRI sequences are provided in Table 1. No bowel preparation was received prior to the MRI examination.

Table 1. MRI parameters.

| MRI Parameter | TSE T2-Weighted Image | | | DWI |
|------------------------|-----------------------|--------------------|------------------|-----------|
| | Sagittal | HR Coronal Oblique | HR Axial Oblique | |
| TR (ms) | 3500 | 3500 | 4000 | 5800 |
| TE (ms) | 91 | 91 | 80 | 96 |
| Slice no | 28 | 25 | 25 | 30 |
| Bandwidth (Hz/pixel) | 391 | 391 | 391 | 1132 |
| FOV (mm) | 220 | 220 | 200 | 250 |
| Slice thickness (mm) | 3 | 4 | 3 | 4 |
| Matrix | 256 × 256 | 256 × 256 | 256 × 256 | 136 × 160 |
| Acquisition time (min) | 4 | 5.5 | 6 | 4.5 |

2.3. Tumor Segmentation and Feature Extraction

Two radiologists (one radiology resident and one senior radiologist with over 10 years of experience in gastrointestinal MRI), blinded to the clinical information and patients' outcome, independently reviewed the MR images, and delineated the rectal tumors. They manually drew regions of interest (ROIs) along the border of the tumor on each consecutive slice of the ADC maps, covering the whole lesion, resulting in a VOI. Cystic, necrotic, or hemorrhagic areas and artifacts were carefully excluded by referring to T2-weighted and diffusion-weighted images as a guide. The segmentation of the tumors was performed using a designated, open source software 3D Slicer, version 4.10.2 (available at: <https://www.slicer.org/>, last accessed on 15 December 2021).

Thereafter, ADC first-order features were automatically extracted from each VOI using the pyRadiomics package, implemented as a plugin into the 3D Slicer software. The following ADC first-order features were extracted from the whole-tumor VOIs: minimum, maximum, mean, median, 10th percentile, 90th percentile, skewness, kurtosis, interquartile range, entropy, energy, uniformity, variance, mean absolute deviation, robust mean absolute deviation, root mean square, and range. A bin width of 25 (standard value in 3D Slicer) was applied before feature extraction. No other preprocessing of the ADC maps was performed. Table 2 provides a brief description for each extracted first-order feature.

Table 2. Description of ADC first-order histogram-based features.

| ADC First-Order Histogram Feature | Description |
|-----------------------------------|--|
| Minimum | The minimum ADC value within the VOI. |
| Maximum | The maximum ADC value within the VOI. |
| Mean | The average ADC value within the VOI. |
| Median | The ADC value below 50% of all ADC voxel values lie. |
| 10th percentile | The ADC value below 10% of all ADC voxel values lie. |
| 90th percentile | The ADC value below 90% of all ADC voxel values lie. |
| Skewness | Measures the asymmetry of the distribution of ADC values around the mean value. |
| Kurtosis | Measures the 'peakedness' of the distribution of ADC values within the VOI. |
| Interquartile range | Measures the spread of the distribution of ADC values, defined as the difference between 75th and 25th percentile. |
| Entropy | Measures the inherent randomness in the ADC values within the VOI. |
| Energy | Measures the squared magnitude of ADC values within the VOI. |
| Uniformity | Measures the homogeneity in the ADC values within the VOI. |
| Variance | Measures squared distances of each ADC value of a histogram from the mean. |

Table 2. Cont.

| ADC First-Order Histogram Feature | Description |
|-----------------------------------|--|
| Mean absolute deviation | Mean distance of all ADC values from the mean value of the image array. |
| Robust mean absolute deviation | Mean distance of all ADC values from the mean value calculated on the subset of image array with ADC in between, or equal to the 10th and 90th percentile. |
| Range | Measures difference between the highest and lowest ADC values. |
| RootMeanSquared | Square root of the mean of all the squared ADC values of the histogram. This feature is another measure of the magnitude of a histogram. |

The histogram plots of ADC values were generated using a python code, provided in Supplementary File S1. Figures 2 and 3 show two examples of tumor segmentation and histogram plots, representative for each subgroup of patients.

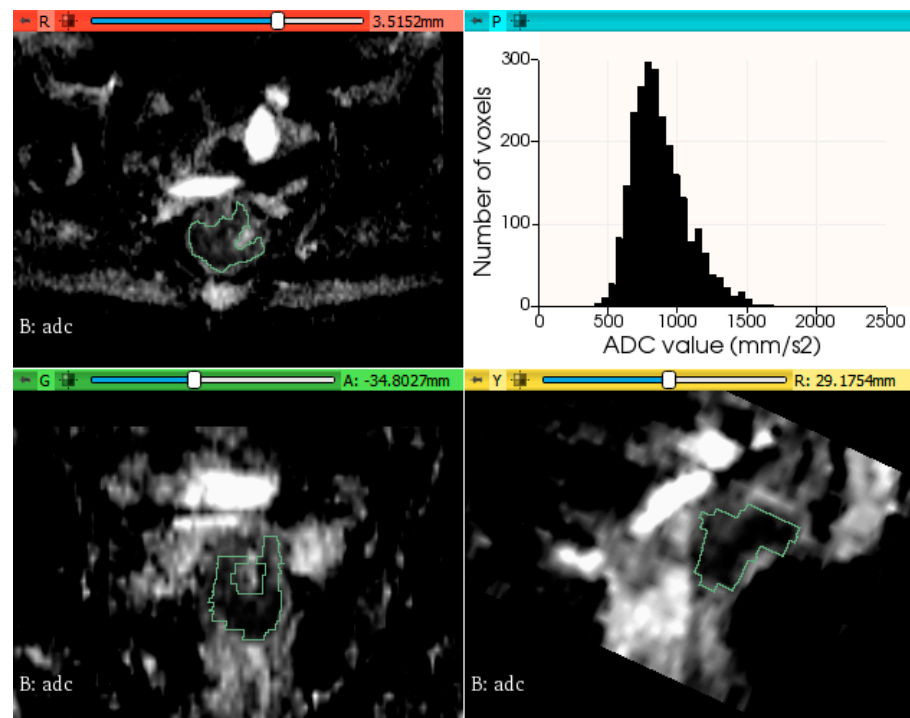


Figure 2. Example of rectal tumor VOI segmentation on ADC map and histogram plot of the ADC values from a patient without metachronous metastases.

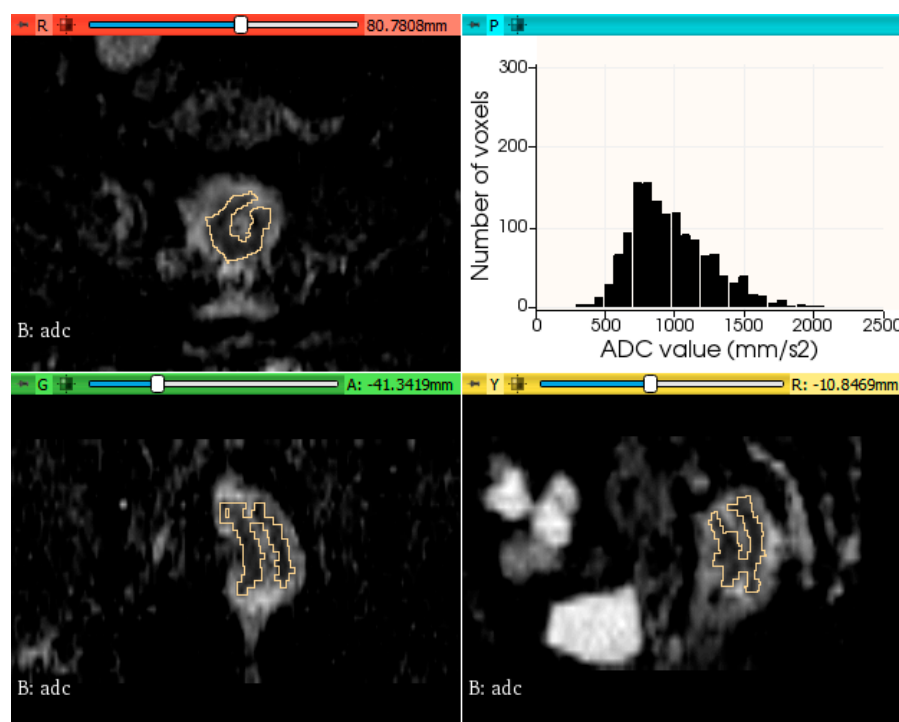


Figure 3. Example of rectal tumor VOI segmentation on ADC map and histogram plot of the ADC values from a patient with metachronous metastases.

2.4. Statistical Analysis

Statistical analysis was performed using commercially available software: MedCalc for Windows, V.14.8 (MedCalc Software, Ostend, Belgium), and SPSS Statistics for Windows, version 18.0 (SPSS Inc., Chicago, IL, USA). Categorical variables are expressed as counts and compared using chi test. Continuous variables are represented as means \pm standard deviation. Normality was tested using the Kolmogorov–Smirnov test.

The inter-reader agreement was evaluated using the intraclass coefficient (ICC) between the features extracted from the radiology resident’s segmentation and senior radiologist’s segmentation. Only features with an ICC \geq 0.75 were selected for further analysis, and they were averaged between the two observers.

The differences in ADC histogram metrics between the two groups (non-metastatic vs. metastatic) were evaluated using independent Student’s *t*-test or non-parametric Mann-Whitney U test, in case of non-normally distributed data.

Receiver operating characteristic (ROC) curve analysis was conducted and area under the curve (AUC), sensitivity (Se), specificity (Sp), positive predictive value (PPV), and negative predictive value (NPV) were calculated to evaluate the diagnostic performance of the individual ADC first-order features for the prediction of metachronous metastases. The optimal cut-off value was chosen according to the Youden index. Using binary logistic regression (enter method), the authors created a combined model, which was also evaluated using ROC curve analysis. ROC curves were compared using the method developed by DeLong et al. A *p*-value of <0.05 was considered statistically significant.

3. Results

Among all 52 enrolled patients with rectal cancer, 15 developed distant metachronous metastases. The mean time interval of follow-up was 24 months. The most common site of metastases was the liver (14 patients). Five subjects developed simultaneous liver and lung metastases and one patient was diagnosed with peritoneal carcinomatosis.

A summary of the clinical and histopathological characteristics of the study population is shown in Table 3. No statistically significant differences of any clinical or histopathological variable were observed between the two groups of patients.

Table 3. Clinical and histopathological characteristics of the study population.

| Variable | Non Metastases (MM-) Group (n = 37) | Metachronous Metastases (MM+) Group (n = 15) | p Value |
|-------------------------------------|-------------------------------------|--|---------|
| Age (years) * | 59.27 ± 11.11 | 61.87 ± 9.85 | 0.43 |
| Gender | | | 0.29 |
| Male | 27 | 8 | |
| Female | 10 | 7 | |
| Tumor length (mm) * | 58.22 ± 19.74 | 53.93 ± 18.57 | 0.47 |
| Tumor differentiation grade | | | 0.41 |
| G1–G2 | 36 | 13 | |
| G3 | 1 | 2 | |
| Clinical tumor stage (cT) | | | 0.98 |
| T2 | 9 | 3 | |
| T3–T4 | 28 | 12 | |
| Clinical nodal stage (cN) | | | 0.93 |
| N1 | 17 | 6 | |
| N2 | 20 | 9 | |
| Mesorectal fascia (MRF) involvement | | | 0.80 |
| Positive | 29 | 12 | |
| Negative | 8 | 3 | |
| Extramural vascular invasion (EMVI) | | | 0.95 |
| Positive | 4 | 1 | |
| Negative | 33 | 14 | |
| Pathological tumor stage (pT) | | | 0.15 |
| pT0–pT2 | 17 | 3 | |
| pT3 | 20 | 12 | |
| Pathological nodal stage (pN) | | | 0.30 |
| pN0 | 27 | 8 | |
| pN1–N2 | 10 | 7 | |

* Results are presented as mean ± standard deviation or number.

The ADC histogram first-order features of the two groups are provided in Table 4. The 90th percentile, interquartile range, entropy, variance, mean absolute deviation, and robust mean absolute deviation were significantly higher among patients with metachronous metastases, compared with the ones without metastases (*p* values ranging between 0.002–0.01). Uniformity was lower in subjects with distant tumor spread. However, there were no significant differences between the two subgroups, regarding the other first-order features.

Table 4. Association of ADC first-order features and the presence of metachronous metastases.

| ADC First-Order Feature | MM- | MM+ | p Value |
|--------------------------------|-------------------------------------|-------------------------------------|---------|
| Minimum $\hat{\wedge}$ | 310.84 ± 193.73 | 243.87 ± 210.26 | 0.28 |
| Maximum $\hat{\wedge}$ | 1972.22 ± 284.54 | 2047.13 ± 294.47 | 0.40 |
| Mean $\hat{\wedge}$ | 927.20 ± 100.45 | 974.48 ± 93.91 | 0.12 |
| Median $\hat{\wedge}$ | 901.96 ± 98.87 | 949.07 ± 104.04 | 0.13 |
| 10th percentile $\hat{\wedge}$ | 679.14 ± 101.11 | 694.65 ± 91.58 | 0.61 |
| 90th percentile $\hat{\wedge}$ | 1210.20 ± 112.90 | 1293.60 ± 103.65 | 0.02 * |
| Skewness | 0.72 ± 0.41 | 0.60 ± 0.29 | 0.32 |
| Kurtosis | 4.52 ± 1.11 | 3.90 ± 0.74 | 0.05 |
| Interquartile Range | 269.62 ± 33.63 | 308.42 ± 51.64 | 0.002 * |
| Entropy | 5.04 ± 0.15 | 5.20 ± 0.22 | 0.005 * |
| Energy | 1,465,303,600.05 ± 1,764,343,232.40 | 1,814,657,493.13 ± 1,913,810,213.47 | 0.53 |

Table 4. Cont.

| ADC First-Order Feature | MM- | MM+ | p Value |
|-------------------------|-----------------------|-----------------------|---------|
| Uniformity | 0.037 ± 0.004 | 0.032 ± 0.005 | 0.004 * |
| Variance | 48,432.81 ± 11,167.16 | 59,287.71 ± 18,590.48 | 0.01 * |
| Mean absolute deviation | 168.38 ± 19.22 | 188.70 ± 29.88 | 0.005 * |
| Robust mean | 112.90 ± 13.60 | 129.40 ± 21.38 | 0.002 * |
| Absolute deviation | | | |
| Range | 1661.38 ± 340.22 | 1803.27 ± 467.76 | 0.23 |
| RootMeanSquared | 953.14 ± 98.66 | 1004.59 ± 92.28 | 0.08 |

* Statistically significant $p < 0.05$. ^ The unit of values is 10^{-6} mm²/s.

Table 5 demonstrates the results of the ROC analysis of ADC parameters for the detection of patients who developed metachronous metastases. The 90th percentile and uniformity showed the best diagnostic performance for predicting the occurrence of metachronous metastases, yielding an AUC of 0.74 [95% CI: 0.60–0.85]. Variance achieved the lowest AUC of 0.65 [95% CI: 0.51–0.78]. The highest sensitivity (80.0%) was achieved by 90th percentile for the cut-off value of 1236.2. Variance reached the highest specificity (86.49%) for the cut-off value of 57046. When comparing the diagnostic performance between individual ADC features, we found a statistically significant difference only between uniformity and variance ($p = 0.03$). Using logistic regression (entry method), we incorporated these seven first-order features into a combined model, which achieved a higher AUC of 0.80 [95% CI: 0.66–0.90]. However, this was only significantly different from the AUC of variance ($p = 0.04$).

Table 5. Diagnostic performance of ADC first-order features for predicting metachronous metastases.

| ADC First-Order Feature | Cut-Off Value | AUC [95% CI] | Se [95% CI] | Sp [95% CI] | PPV [95% CI] | NPV [95% CI] |
|--------------------------------|---------------|------------------|-------------------|-------------------|-------------------|------------------|
| 90th percentile | >1236.2 * | 0.74 [0.60–0.85] | 80.0 [51.9–95.7] | 64.86 [47.5–79.8] | 48.0 [27.8–68.7] | 88.9 [70.8–97.6] |
| Interquartile range | >287.25 | 0.72 [0.58–0.83] | 73.33 [38.4–88.2] | 75.68 [58.8–88.2] | 52.6 [28.9–75.6] | 84.8 [68.1–94.9] |
| Entropy | >5.125 | 0.7 [0.56–0.82] | 60.00 [32.3–83.7] | 83.78 [68.0–93.8] | 60.00 [32.3–83.7] | 83.8 [68.0–93.8] |
| Uniformity | ≤0.0344 | 0.74 [0.60–0.85] | 73.33 [44.9–92.2] | 78.38 [61.8–90.2] | 57.9 [33.5–79.7] | 87.9 [71.8–96.6] |
| Variance | >57046 | 0.65 [0.51–0.78] | 53.33 [26.6–78.7] | 86.49 [71.2–95.5] | 61.5 [31.6–86.1] | 82.1 [66.5–92.5] |
| Mean absolute deviation | >175.89 | 0.70 [0.55–0.82] | 66.67 [38.4–88.2] | 78.38 [61.8–90.2] | 55.6 [30.8–78.5] | 85.3 [68.9–95.0] |
| Robust mean absolute deviation | >119.2689 | 0.73 [0.59–0.84] | 73.33 [44.9–92.2] | 78.38 [61.8–90.2] | 57.9 [33.5–79.7] | 87.9 [71.8–96.6] |

* The unit of values is 10^{-6} mm²/s.

4. Discussion

Our study evaluated the potential of histogram metrics, derived from pretreatment ADC maps, to predict the occurrence of metachronous metastases in patients diagnosed with rectal cancer. In the past years, there has been an increased interest in the field of medical imaging texture analysis for lesion characterization, therapy guidance, and tumor prognosis.

Regarding rectal cancer outcome, the majority of papers focused on predicting tumor response to nCRT, using a single MRI sequence (T2-weighted images or ADC maps) or multiparametric approach [33–35]. Only a few studies chose the occurrence of metachronous

metastases as the endpoint of their research, most of them obtaining predicting models, based on radiomics features extracted from T2 weighted images [36–38].

For the current research, we chose to not include all the radiomics features extracted from the tumor, but only first-order features derived from histogram. In spite of the possible advantage of higher-order statistics to better reflect intratumoral heterogeneity, previous studies have demonstrated that, with respect to rectal cancer, first-order texture parameters proved to be more stable and sufficiently robust, being less sensitive to interobserver variability and image processing [39,40].

The association between whole-rectal tumor ADC histogram parameters and different clinical pathologic prognostic factors has been the main subject of many papers, however, with conflicting factors [31,32,41–48]. Regarding pT stage, a well-recognized powerful prognostic factor, there are several studies that demonstrate significantly lower values of ADC histogram metrics in tumors with pT1-T2 stages [32,41,49]. Conversely, other investigations found no significant differences in ADC histogram percentiles among different pT stages [50]. Additionally, inconsistent results are reported for the role of pretreatment ADC histogram metrics in predicting treatment response to nCRT. The investigations of Liang et al. [51] and Palmisano et al. [52] obtained AUCs between 0.82 and 0.89 for histogram parameters, such as mean, median, and 75th percentile, to distinguish between pCR and nonPCR, while the studies of Choi et al. [48] and Nougaret et al. [53] found no benefit in any of the ADC histogram metrics for pretreatment prediction of response. The recent meta-analysis of Surov et al. concluded that the mean ADC cannot predict histopathological features and response to nCRT in rectal cancer [26]. Additionally, the results of van Heeswijk et al. [47] and Chidambaram et al. [46] revealed that ADC histogram analyses of rectal cancer were not beneficial to obtaining prognostic information. In our study, we did not find any significant difference in mean ADC between metastatic vs. nonmetastatic tumors. Therefore, our observations support the conclusions of these latter studies, suggesting that ADC mean value has no additional prognostic value.

However, in this current research, ADC 90th percentile showed the best diagnostic performance in predicting metachronous metastases. Contrary to our expectations, patients who developed MM had significantly higher values of ADC in the 90th percentile. One possible explanation for this finding might be that more aggressive cancers may contain many invisible areas of cystic and necrotic components, which cannot be completely excluded using manual segmentation. Similar results, with higher ADC percentiles, in more aggressive lesions, have also been reported in other oncological investigations [54,55].

All the studies mentioned above included in their analysis only ADC mean, histogram percentiles \pm skewness, and kurtosis. In addition, we also assessed the role of other first order histogram-based features, such as entropy, uniformity, variance, mean absolute deviation, etc., for the differentiation of tumors, which developed metachronous metastases versus the ones without distant spread. Our results suggest that evaluating all the first-order texture features may bring additional information and improve the prognostic ability of ADC maps. Entropy specifies the randomness in the image values, and it measures the average amount of information required to encode the image values [56]. Uniformity is a measure of the sum of the squares of each intensity value, and it indicates the homogeneity of the image array [56]. A lower value of uniformity, as well as a high value of entropy, indicate greater heterogeneity of the lesion [57]. According to our results, prognostically unfavorable tumors have significantly lower uniformity and higher entropy values and are, therefore, more heterogeneous. Similar findings have been reported in previous studies. Regarding entropy, several authors revealed rectal tumors with higher pT stages showing significantly higher values of ADC entropy, reporting AUCs between 0.67–0.74 [31,42,57,58]. As for uniformity, the results of Meng et al. showed significantly lower ADC uniformity values in rectal tumors, without a complete response to nCRT, obtaining an AUC of 0.69 [59]. Additionally, Lu et al. reported lower uniformity in pT3-T4 rectal cancers, compared to pT1-T2 lesions, with an AUC of 0.63 [57]. In our study, each statistically significant first-order feature achieved an individual AUC between 0.65–0.74 for differentiating MM+

from MM-tumors, while the combined model increased the prognostic efficacy, yielding a moderate AUC of 0.8.

To the best of our knowledge, this is the first study to investigate the association of all first-order texture features, derived from ADC maps, with the occurrence of metachronous metastases. The research of Yu et al. evaluated the correlation between ADC histogram parameters and distant metastases (DM) from rectal cancer; however, they considered DM as both synchronous and metachronous metastases, and they did not include in their analysis all the first-order histogram features [60]. Conversely to our results, they found significantly higher kurtosis values of tumors with DM. Another paper of Chidambaram et al. reported a significant correlation between skewness and disease progression; however, in their investigation, kurtosis did not differ significantly between the different subgroups [46]. This discrepancy between studies might have resulted from the small number of patients included.

The current study has some limitations. First of all, its retrospective nature might have led to unintended selection bias. Secondly, many patients did not undergo a proper oncological follow-up, reducing our study population. The MRI examinations were selected from a single center, lacking multicenter validation. Additionally, we included only first-order features, derived from ADC maps, and the role of other imaging sequences may be investigated in future research.

5. Conclusions

Our study suggests that first-order histograms that derive features extracted from pre-treatment ADC maps might represent a potential imaging biomarker to predict metachronous metastases of rectal cancer. However, these results were obtained using a small population and need to be externally validated in larger, multicentric, prospective studies.

Supplementary Materials: The following supporting information can be downloaded at: <https://www.mdpi.com/article/10.3390/biology11030452/s1>, Supplementary File S1: Python code for generation of histogram plot.

Author Contributions: Conceptualization, B.B., L.P., C.C. and M.M.B.; methodology, B.B., L.P. and C.C.; formal analysis, B.B. and D.S.F.; investigation, B.B., A.L. and C.C.; resources, C.B., A.L., C.C. and D.S.F.; data curation, B.B.; writing—original draft preparation, B.B.; writing—review and editing, C.B., A.L. and C.C.; visualization, L.P. and B.B.; supervision, M.M.B.; project administration, M.M.B. All authors have read and agreed to the published version of the manuscript.

Funding: This research received no external funding.

Institutional Review Board Statement: The study was conducted according to the guidelines of the Declaration of Helsinki and approved by the Institutional Ethics Committee of Regional Institute of Gastroenterology and Hepatology “Prof. Dr Octavian Fodor” Cluj-Napoca (protocol code 5337, date of approval 12 June 2020).

Informed Consent Statement: Patient consent was waived, due to the retrospective nature of the study.

Data Availability Statement: Data available on request due to privacy restrictions.

Conflicts of Interest: The authors declare no conflict of interest.

References

1. Sung, H.; Ferlay, J.; Siegel, R.L.; Laversanne, M.; Soerjomataram, I.; Jemal, A.; Bray, F. Global Cancer Statistics 2020: GLOBOCAN Estimates of Incidence and Mortality Worldwide for 36 Cancers in 185 Countries. *CA Cancer J. Clin.* **2021**, *71*, 209–249. [[CrossRef](#)]
2. Siegel, R.L.; Miller, K.D.; Fuchs, H.E.; Jemal, A. Cancer Statistics, 2021. *CA Cancer J. Clin.* **2021**, *71*, 7–33. [[CrossRef](#)]
3. Dekker, E.; Tanis, P.J.; Vleugels, J.L.A.; Kasi, P.M.; Wallace, M.B. Colorectal Cancer. *Lancet* **2019**, *394*, 1467–1480. [[CrossRef](#)]
4. Edge, S.B.; Compton, C.C. The American Joint Committee on Cancer: The 7th Edition of the AJCC Cancer Staging Manual and the Future of TNM. *Ann. Surg. Oncol.* **2010**, *17*, 1471–1474. [[CrossRef](#)]

5. Valentini, V.; van Stiphout, R.G.P.M.; Lammering, G.; Gambacorta, M.A.; Barba, M.C.; Bebenek, M.; Bonnetain, F.; Bosset, J.F.; Bujko, K.; Cionini, L.; et al. Selection of Appropriate End-Points (PCR vs. 2yDFS) for Tailoring Treatments with Prediction Models in Locally Advanced Rectal Cancer. *Radiother. Oncol.* **2015**, *114*, 302–309. [[CrossRef](#)]
6. Sauer, R.; Liersch, T.; Merkel, S.; Fietkau, R.; Hohenberger, W.; Hess, C.; Becker, H.; Raab, H.R.; Villanueva, M.T.; Witzigmann, H.; et al. Preoperative versus Postoperative Chemoradiotherapy for Locally Advanced Rectal Cancer: Results of the German CAO/ARO/AIO-94 Randomized Phase III Trial after a Median Follow-up of 11 Years. *J. Clin. Oncol.* **2012**, *30*, 1926–1933. [[CrossRef](#)]
7. Peeters, K.C.M.J.; Marijnen, C.A.M.; Nagtegaal, I.D.; Kranenbarg, E.K.; Putter, H.; Wiggers, T.; Rutten, H.; Pahlman, L.; Glimelius, B.; Leer, J.W.; et al. The TME Trial after a Median Follow-up of 6 Years: Increased Local Control but No Survival Benefit in Irradiated Patients with Resectable Rectal Carcinoma. *Ann. Surg.* **2007**, *246*, 693–701. [[CrossRef](#)]
8. Manfredi, S.; Lepage, C.; Hatem, C.; Coatmeur, O.; Faivre, J.; Bouvier, A.M. Epidemiology and Management of Liver Metastases from Colorectal Cancer. *Ann. Surg.* **2006**, *244*, 254–259. [[CrossRef](#)]
9. Van Gijn, W.; Marijnen, C.A.M.; Nagtegaal, I.D.; Kranenbarg, E.M.K.; Putter, H.; Wiggers, T.; Rutten, H.J.T.; Pahlman, L.; Glimelius, B.; van de Velde, C.J.H. Preoperative Radiotherapy Combined with Total Mesorectal Excision for Resectable Rectal Cancer: 12-Year Follow-up of the Multicentre, Randomised Controlled TME Trial. *Lancet Oncol.* **2011**, *12*, 575–582. [[CrossRef](#)]
10. Taylor, F.G.M.; Quirke, P.; Heald, R.J.; Moran, B.J.; Blomqvist, L.; Swift, I.R.; Sebag-Montefiore, D.; Tekkis, P.; Brown, G. Preoperative Magnetic Resonance Imaging Assessment of Circumferential Resection Margin Predicts Disease-Free Survival and Local Recurrence: 5-Year Follow-up Results of the MERCURY Study. *J. Clin. Oncol.* **2014**, *32*, 34–43. [[CrossRef](#)]
11. Maas, M.; Nelemans, P.J.; Valentini, V.; Crane, C.H.; Capirci, C.; Rödel, C.; Nash, G.M.; Kuo, L.J.; Glynne-Jones, R.; García-Aguilar, J.; et al. Adjuvant Chemotherapy in Rectal Cancer: Defining Subgroups Who May Benefit after Neoadjuvant Chemoradiation and Resection: A Pooled Analysis of 3313 Patients. *Int. J. Cancer* **2015**, *137*, 212–220. [[CrossRef](#)]
12. Zhang, H.; Huang, Y.; Sun, G.; Zheng, K.; Lou, Z.; Gao, X.-H.; Hao, L.-Q.; Liu, L.-J.; Meng, R.-G.; Zhang, W. Rectal Cancer Patients with Downstaging after Neoadjuvant Chemoradiotherapy and Radical Resection Do Not Benefit from Adjuvant Chemotherapy. *Ann. Transl. Med.* **2020**, *8*, 743. [[CrossRef](#)]
13. Dossa, F.; Acuna, S.A.; Rickles, A.S.; Berho, M.; Wexner, S.D.; Quereshey, F.A.; Baxter, N.N.; Chadi, S.A. Association Between Adjuvant Chemotherapy and Overall Survival in Patients with Rectal Cancer and Pathological Complete Response After Neoadjuvant Chemotherapy and Resection. *JAMA Oncol.* **2018**, *4*, 930–937. [[CrossRef](#)]
14. Polanco, P.M.; Mokdad, A.A.; Zhu, H.; Choti, M.A.; Huerta, S. Association of Adjuvant Chemotherapy with Overall Survival in Patients with Rectal Cancer and Pathologic Complete Response Following Neoadjuvant Chemotherapy and Resection. *JAMA Oncol.* **2018**, *4*, 938–943. [[CrossRef](#)]
15. Breugom, A.J.; Swets, M.; Bosset, J.F.; Collette, L.; Sainato, A.; Cionini, L.; Glynne-Jones, R.; Counsell, N.; Bastiaannet, E.; van den Broek, C.B.M.; et al. Adjuvant Chemotherapy after Preoperative (Chemo)Radiotherapy and Surgery for Patients with Rectal Cancer: A Systematic Review and Meta-Analysis of Individual Patient Data. *Lancet. Oncol.* **2015**, *16*, 200–207. [[CrossRef](#)]
16. Chung, M.J.; Lee, J.H.; Lee, J.H.; Kim, S.H.; Song, J.H.; Jeong, S.; Yu, M.; Nam, T.K.; Jeong, J.U.; Jang, H.S. Adjuvant Chemotherapy in Rectal Cancer Patients Treated with Preoperative Chemoradiation and Total Mesorectal Excision: A Multicenter and Retrospective Propensity-Score Matching Study. *Int. J. Radiat. Oncol. Biol. Phys.* **2019**, *103*, 438–448. [[CrossRef](#)]
17. Benson, A.B.; Venook, A.P.; Al-Hawary, M.M.; Cederquist, L.; Chen, Y.J.; Ciombor, K.K.; Cohen, S.; Cooper, H.S.; Deming, D.; Engstrom, P.F.; et al. Rectal Cancer, Version 2.2018 Clinical Practice Guidelines in Oncology. *JNCCN J. Natl. Compr. Cancer Netw.* **2018**, *16*, 874–901. [[CrossRef](#)]
18. Brown, G.; Radcliffe, A.G.; Newcombe, R.G.; Dallimore, N.S.; Bourne, M.W.; Williams, G.T. Preoperative Assessment of Prognostic Factors in Rectal Cancer Using High-Resolution Magnetic Resonance Imaging. *Br. J. Surg.* **2003**, *90*, 355–364. [[CrossRef](#)]
19. Lee, E.S.; Kim, M.J.; Park, S.C.; Hur, B.Y.; Hyun, J.H.; Chang, H.J.; Baek, J.Y.; Kim, S.Y.; Kim, D.Y.; Oh, J.H. Magnetic Resonance Imaging-Detected Extramural Venous Invasion in Rectal Cancer before and after Preoperative Chemoradiotherapy: Diagnostic Performance and Prognostic Significance. *Eur. Radiol.* **2018**, *28*, 496–505. [[CrossRef](#)]
20. Cienfuegos, J.A.; Rotellar, F.; Baixauli, J.; Beorlegui, C.; Sola, J.J.; Arbea, L.; Pastor, C.; Arredondo, J.; Hernández-Lizoáin, J.L. Impact of Perineural and Lymphovascular Invasion on Oncological Outcomes in Rectal Cancer Treated with Neoadjuvant Chemoradiotherapy and Surgery. *Ann. Surg. Oncol.* **2015**, *22*, 916–923. [[CrossRef](#)]
21. Ramón y Cajal, S.; Sesé, M.; Capdevila, C.; Aasen, T.; de Mattos-Arruda, L.; Diaz-Cano, S.J.; Hernández-Losa, J.; Castellví, J. Clinical Implications of Intratumor Heterogeneity: Challenges and Opportunities. *J. Mol. Med.* **2020**, *98*, 161–177. [[CrossRef](#)]
22. Jamal-Hanjani, M.; Quezada, S.A.; Larkin, J.; Swanton, C. Translational Implications of Tumor Heterogeneity. *Clin. Cancer Res.* **2015**, *21*, 1258–1266. [[CrossRef](#)]
23. O'Connor, J.P.B.; Rose, C.J.; Waterton, J.C.; Carano, R.A.D.; Parker, G.J.M.; Jackson, A. Imaging Intratumor Heterogeneity: Role in Therapy Response, Resistance, and Clinical Outcome. *Clin. Cancer Res.* **2015**, *21*, 249–257. [[CrossRef](#)]
24. Surov, A.; Meyer, H.J.; Wienke, A. Associations between Apparent Diffusion Coefficient (ADC) and KI 67 in Different Tumors: A Meta-Analysis. Part 1: ADC Mean. *Oncotarget* **2017**, *8*, 75434–75444. [[CrossRef](#)]
25. Surov, A.; Meyer, H.J.; Wienke, A. Correlation between Apparent Diffusion Coefficient (ADC) and Cellularity Is Different in Several Tumors: A Meta-Analysis. *Oncotarget* **2017**, *8*, 59492–59499. [[CrossRef](#)]

26. Surov, A.; Pech, M.; Powerski, M.; Woidacki, K.; Wienke, A. Pretreatment Apparent Diffusion Coefficient Cannot Predict Histopathological Features and Response to Neoadjuvant Radiochemotherapy in Rectal Cancer: A Meta-Analysis. *Dig. Dis.* **2021**, *40*, 33–49. [[CrossRef](#)]
27. Just, N. Improving Tumour Heterogeneity MRI Assessment with Histograms. *Br. J. Cancer* **2014**, *111*, 2205–2213. [[CrossRef](#)]
28. Donati, O.F.; Mazaheri, Y.; Afaq, A.; Vargas, H.A.; Zheng, J.; Moskowitz, C.S.; Hricak, H.; Akin, O. Prostate Cancer Aggressiveness: Assessment with Whole-Lesion Histogram Analysis of the Apparent Diffusion Coefficient. *Radiology* **2014**, *271*, 143–152. [[CrossRef](#)]
29. Park, G.E.; Kim, S.H.; Kim, E.J.; Kang, B.J.; Park, M.S. Histogram Analysis of Volume-Based Apparent Diffusion Coefficient in Breast Cancer. *Acta Radiol.* **2017**, *58*, 1294–1302. [[CrossRef](#)]
30. Xue, H.; Ren, C.; Yang, J.; Sun, Z.; Li, S.; Jin, Z.; Shen, K.; Zhou, W. Histogram Analysis of Apparent Diffusion Coefficient for the Assessment of Local Aggressiveness of Cervical Cancer. *Arch. Gynecol. Obstet.* **2014**, *290*, 341–348. [[CrossRef](#)]
31. Zhang, K.; Zheng, Y.; Huang, H.; Lei, J. Preliminary Study on Predicting Pathological Staging and Immunohistochemical Markers of Rectal Cancer Based on ADC Histogram Analysis. *Acad. Radiol.* **2021**, *28* (Suppl. 1), S184–S191. [[CrossRef](#)] [[PubMed](#)]
32. Peng, Y.; Tang, H.; Hu, X.; Shen, Y.; Kamel, I.; Li, Z.; Hu, D. Rectal Cancer Invasiveness: Whole-Lesion Diffusion-Weighted Imaging (DWI) Histogram Analysis by Comparison of Reduced Field-of-View and Conventional DWI Techniques. *Sci. Rep.* **2019**, *9*, 18760. [[CrossRef](#)] [[PubMed](#)]
33. Staal, F.C.R.; van der Reijnd, D.J.; Taghavi, M.; Lambregts, D.M.J.; Beets-Tan, R.G.H.; Maas, M. Radiomics for the Prediction of Treatment Outcome and Survival in Patients with Colorectal Cancer: A Systematic Review. *Clin. Colorectal Cancer* **2021**, *20*, 52–71. [[CrossRef](#)] [[PubMed](#)]
34. Di Re, A.M.; Sun, Y.; Sundaresan, P.; Hau, E.; Toh, J.W.T.; Gee, H.; Or, M.; Haworth, A. MRI Radiomics in the Prediction of Therapeutic Response to Neoadjuvant Therapy for Locoregionally Advanced Rectal Cancer: A Systematic Review. *Expert Rev. Anticancer Ther.* **2021**, *21*, 425–449. [[CrossRef](#)]
35. Nardone, V.; Boldrini, L.; Grassi, R.; Franceschini, D.; Morelli, I.; Becherini, C.; Loi, M.; Greto, D.; Desideri, I. Radiomics in the Setting of Neoadjuvant Radiotherapy: A New Approach for Tailored Treatment. *Cancers* **2021**, *13*, 3590. [[CrossRef](#)]
36. Chiloiro, G.; Rodriguez-Carnero, P.; Lenkowicz, J.; Casà, C.; Masciocchi, C.; Boldrini, L.; Cusumano, D.; Dinapoli, N.; Meldolesi, E.; Carano, D.; et al. Delta Radiomics Can Predict Distant Metastases in Locally Advanced Rectal Cancer: The Challenge to Personalize the Cure. *Front. Oncol.* **2020**, *10*, 595012. [[CrossRef](#)]
37. Jeon, S.H.; Song, C.; Chie, E.K.; Kim, B.; Kim, Y.H.; Chang, W.; Lee, Y.J.; Chung, J.H.; Chung, J.B.; Lee, K.W.; et al. Delta-Radiomics Signature Predicts Treatment Outcomes after Preoperative Chemoradiotherapy and Surgery in Rectal Cancer. *Radiat. Oncol.* **2019**, *14*, 43. [[CrossRef](#)]
38. Liang, M.; Cai, Z.; Zhang, H.; Huang, C.; Meng, Y.; Zhao, L.; Li, D.; Ma, X.; Zhao, X. Machine Learning-Based Analysis of Rectal Cancer MRI Radiomics for Prediction of Metachronous Liver Metastases. *Acad. Radiol.* **2019**, *26*, 1495–1504. [[CrossRef](#)]
39. Traverso, A.; Kazmierski, M.; Shi, Z.; Kalendralis, P.; Welch, M.; Nissen, H.D.; Jaffray, D.; Dekker, A.; Wee, L. Stability of Radiomic Features of Apparent Diffusion Coefficient (ADC) Maps for Locally Advanced Rectal Cancer in Response to Image Pre-Processing. *Phys. Med.* **2019**, *61*, 44–51. [[CrossRef](#)]
40. Gourtsoyianni, S.; Doumou, G.; Prezzi, D.; Taylor, B.; Stirling, J.J.; Taylor, N.J.; Siddique, M.; Cook, G.J.R.; Glynne-Jones, R.; Goh, V. Primary Rectal Cancer: Repeatability of Global and Local-Regional MR Imaging Texture Features. *Radiology* **2017**, *284*, 552–561. [[CrossRef](#)]
41. Cui, Y.; Yang, X.; Du, X.; Zhuo, Z.; Xin, L.; Cheng, X. Whole-Tumour Diffusion Kurtosis MR Imaging Histogram Analysis of Rectal Adenocarcinoma: Correlation with Clinical Pathologic Prognostic Factors. *Eur. Radiol.* **2018**, *28*, 1485–1494. [[CrossRef](#)] [[PubMed](#)]
42. Liu, L.; Liu, Y.; Xu, L.; Li, Z.; Lv, H.; Dong, N.; Li, W.; Yang, Z.; Wang, Z.; Jin, E. Application of Texture Analysis Based on Apparent Diffusion Coefficient Maps in Discriminating Different Stages of Rectal Cancer. *J. Magn. Reson. Imaging* **2017**, *45*, 1798–1808. [[CrossRef](#)]
43. Peng, Y.; Tang, H.; Meng, X.; Shen, Y.; Hu, D.; Kamel, I.; Li, Z. Histological Grades of Rectal Cancer: Whole-Volume Histogram Analysis of Apparent Diffusion Coefficient Based on Reduced Field-of-View Diffusion-Weighted Imaging. *Quant. Imaging Med. Surg.* **2020**, *10*, 243–256. [[CrossRef](#)] [[PubMed](#)]
44. Li, W.; Jiang, Z.; Guan, Y.; Chen, Y.; Huang, X.; Liu, S.; He, J.; Zhou, Z.; Ge, Y. Whole-Lesion Apparent Diffusion Coefficient First- and Second-Order Texture Features for the Characterization of Rectal Cancer Pathological Factors. *J. Comput. Assist. Tomogr.* **2018**, *42*, 642–647. [[CrossRef](#)] [[PubMed](#)]
45. Li, J.; Zhou, Y.; Wang, X.; Yu, Y.; Zhou, X.; Luan, K. Histogram Analysis of Diffusion-Weighted Magnetic Resonance Imaging as a Biomarker to Predict Lymph Node Metastases in T3 Stage Rectal Carcinoma. *Cancer Manag. Res.* **2021**, *13*, 2983–2993. [[CrossRef](#)]
46. Chidambaram, V.; Brierley, J.D.; Cummings, B.; Bhayana, R.; Menezes, R.J.; Kennedy, E.D.; Kirsch, R.; Jhaveri, K.S. Investigation of Volumetric Apparent Diffusion Coefficient Histogram Analysis for Assessing Complete Response and Clinical Outcomes Following Pre-Operative Chemoradiation Treatment for Rectal Carcinoma. *Abdom. Radiol.* **2017**, *42*, 1310–1318. [[CrossRef](#)]
47. Van Heeswijk, M.M.; Lambregts, D.M.J.; Maas, M.; Lahaye, M.J.; Ayas, Z.; Slenter, J.M.G.M.; Beets, G.L.; Bakers, F.C.H.; Beets-Tan, R.G.H. Measuring the Apparent Diffusion Coefficient in Primary Rectal Tumors: Is There a Benefit in Performing Histogram Analyses? *Abdom. Radiol.* **2017**, *42*, 1627–1636. [[CrossRef](#)]
48. Choi, M.H.; Oh, S.N.; Rha, S.E.; Choi, J.I.; Lee, S.H.; Jang, H.S.; Kim, J.G.; Grimm, R.; Son, Y. Diffusion-Weighted Imaging: Apparent Diffusion Coefficient Histogram Analysis for Detecting Pathologic Complete Response to Chemoradiotherapy in Locally Advanced Rectal Cancer. *J. Magn. Reson. Imaging* **2016**, *44*, 212–220. [[CrossRef](#)]

49. Xie, H.; Wu, G. Application of Diffusion Kurtosis Imaging and Histogram Analysis for Assessing Preoperative Stages of Rectal Cancer. *Gastroenterol. Res. Pract.* **2018**, *2018*, 9786932. [[CrossRef](#)]
50. Tang, C.; Lin, M.B.; Xu, J.L.; Zhang, L.H.; Zuo, X.M.; Zhang, Z.S.; Liu, M.X.; Xu, J.M. Are ADC Values of Readout-Segmented Echo-Planar Diffusion-Weighted Imaging (RESOLVE) Correlated with Pathological Prognostic Factors in Rectal Adenocarcinoma? *World J. Surg. Oncol.* **2018**, *16*, 138. [[CrossRef](#)]
51. Liang, C.Y.; Chen, M.D.; Zhao, X.X.; Yan, C.G.; Mei, Y.J.; Xu, Y.K. Multiple Mathematical Models of Diffusion-Weighted Magnetic Resonance Imaging Combined with Prognostic Factors for Assessing the Response to Neoadjuvant Chemotherapy and Radiation Therapy in Locally Advanced Rectal Cancer. *Eur. J. Radiol.* **2019**, *110*, 249–255. [[CrossRef](#)]
52. Palmisano, A.; Di Chiara, A.; Esposito, A.; Rancoita, P.M.V.; Fiorino, C.; Passoni, P.; Albarello, L.; Rosati, R.; del Maschio, A.; de Cobelli, F. MRI Prediction of Pathological Response in Locally Advanced Rectal Cancer: When Apparent Diffusion Coefficient Radiomics Meets Conventional Volumetry. *Clin. Radiol.* **2020**, *75*. [[CrossRef](#)] [[PubMed](#)]
53. Nougaret, S.; Vargas, H.A.; Lakhman, Y.; Sudre, R.; Do, R.K.G.; Bibeau, F.; Azria, D.; Assenat, E.; Molinari, N.; Pierredon, M.A.; et al. Intravoxel Incoherent Motion-Derived Histogram Metrics for Assessment of Response after Combined Chemotherapy and Radiation Therapy in Rectal Cancer: Initial Experience and Comparison between Single-Section and Volumetric Analyses. *Radiology* **2016**, *280*, 446–454. [[CrossRef](#)] [[PubMed](#)]
54. Kang, Y.; Choi, S.H.; Kim, Y.J.; Kim, K.G.; Sohn, C.H.; Kim, J.H.; Yun, T.J.; Chang, K.H. Gliomas: Histogram Analysis of Apparent Diffusion Coefficient Maps with Standard- or High-b-Value Diffusion-Weighted MR Imaging—Correlation with Tumor Grade. *Radiology* **2011**, *261*, 882–890. [[CrossRef](#)] [[PubMed](#)]
55. Takahashi, M.; Kozawa, E.; Tanisaka, M.; Hasegawa, K.; Yasuda, M.; Sakai, F. Utility of Histogram Analysis of Apparent Diffusion Coefficient Maps Obtained Using 3.0T MRI for Distinguishing Uterine Carcinosarcoma from Endometrial Carcinoma. *J. Magn. Reson. Imaging* **2016**, *43*, 1301–1307. [[CrossRef](#)] [[PubMed](#)]
56. Radiomic Features—Pyradiomics v3.0.1.post11+g03d23f7 Documentation. Available online: <https://pyradiomics.readthedocs.io/en/latest/features.html#module-radiomics.firstorder> (accessed on 31 December 2021).
57. Lu, Z.; Wang, L.; Xia, K.; Jiang, H.; Weng, X.; Jiang, J.; Wu, M. Prediction of Clinical Pathologic Prognostic Factors for Rectal Adenocarcinoma: Volumetric Texture Analysis Based on Apparent Diffusion Coefficient Maps. *J. Med. Syst.* **2019**, *43*, 331. [[CrossRef](#)]
58. Lu, Z.H.; Jiang, H.; Xia, K.J.; Jiang, J.L.; Wu, M. Textural Differences Based on Apparent Diffusion Coefficient Maps for Discriminating PT3 Subclasses of Rectal Adenocarcinoma. *World J. Clin. Cases* **2021**, *9*, 6987. [[CrossRef](#)] [[PubMed](#)]
59. Meng, Y.; Zhang, C.; Zou, S.; Zhao, X.; Xu, K.; Zhang, H.; Zhou, C. MRI Texture Analysis in Predicting Treatment Response to Neoadjuvant Chemoradiotherapy in Rectal Cancer. *Oncotarget* **2018**, *9*, 11999–12008. [[CrossRef](#)]
60. Yu, J.; Huang, D.Y.; Li, Y.; Dai, X.; Shi, H.-B. Correlation of Standard Diffusion-Weighted Imaging and Diffusion Kurtosis Imaging with Distant Metastases of Rectal Carcinoma. *J. Magn. Reson. Imaging* **2016**, *44*, 221–229. [[CrossRef](#)]